Materials Research. 2016; 19(Suppl. 1): 103-112
DOI: http://dx.doi.org/10.1590/1980-5373-MR-2015-0667

Study of the Adsorption of Arsenic (III and V) by Magnetite Nanoparticles Synthetized via AACVD

Blanca Elizabeth Monárrez-Cordero[a], Patricia Amézaga-Madrid[a]*, César Cutberto Leyva-Porras[a], Pedro Pizá-Ruiz[a], Mario Miki-Yoshida[a]

[a] *Departamento de Física de Materiales, Centro de Investigación en Materiales Avanzados S.C., Miguel de Cervantes, 120, Chihuahua, Chihuahua, CP 31136, México*

Received: November 4, 2015; Revised: October 5, 2016; Accepted: November 21, 2016

Globally, water pollution is mainly caused by the presence of heavy metals and metalloids such as arsenic. The majority of the techniques employed in the removal are of low efficiency and high cost. Therefore, in this work it is presented the adsorption processes of arsenic (As III and V) ions employing magnetite nanoparticles (MNPs) synthesized by the aerosol assisted chemical vapor deposition (AACVD) process. The adsorption efficiency was determined at different times and concentrations. The remaining As concentration in the solutions was analyzed by atomic absorption spectroscopy. The adsorbed As ions on the surface of the NMPs was analyzed by high resolution transmission electron microscopy. The results showed an overall removal efficiency of 87% for As^{+3} and 98% for As^{+5}, in a contact time of 15 minutes. Results suggested the use of NMPs as a promising alternative in the removal of As ions in water.

Keywords: *AACVD, MNPs, adsorption isotherms, physisorption process*

1. Introduction

Heavy metals such as lead[1], mercury[1], cadmium[2], chromium[3], nickel[4] and arsenic metalloid[5], are found naturally in the earth's crust; eventually these heavy metals can become contaminants in the air, surface water, groundwater, soil and other aquatic environments. In recent decades, the aquatic environment has been exposed to a large contamination mainly caused by the continuous discharges of pollutants containing heavy metals produced from anthropogenic sources[2]. When these metals reach the food chain, generate a high health risk for the living beings and humanity, because they can accumulate in living tissues causing various disorders and diseases as skin diseases, kidney cancer and even incomplete embryonic development during pregnancy[6,7]. Thus, for this reason, most of the health agencies in the world have decided to reduce the maximum concentration of these toxic ions established in the international norms.In the case of arsenic, it is present in large quantities of groundwater and effluents worldwide, with an allowed maximum limit[8] of 0.01 mg L^{-1}. In natural water bodies, As is found as hydrogen arsenate (H_3AsO_4) and arsenic acid (H_3AsO_3), which at oxidizing or reducing conditions produce As^{+5} and As^{+3} ions, respectively[9]. From these ions, As^{+3} is more toxic. The mobility and bioavailability of these ions largely depend on the adsorption/desorption process of As within the soil and the pH conditions in groundwater[10,11]. The treatment techniques include methodologies such as oxidation, precipitation and co-precipitation[12,13], inverse osmosis[14], and ion exchange[15]. These techniques employ solid adsorbents particles for immobilizing the As ions such as alumina, mineral oxides, active carbon, polymer resins and zeolites[16]. Additionally, when both As ions are presented in the water fluent, the removal process becomes more complex, since As^{+3} must be first oxidized into As^{+5}. Clearly, this increases the overall cost for decontamination of water. Thus, there is a growing interest in the development of low cost methodologies for water treatment, especially for As ions. Consequently, in recent years several adsorbents based on nanometric-scale oxides have been synthesized and tested (TiO_2, Fe_2O_3, Fe_3O_4)[17-21]. Among these oxides, iron oxides have been widely employed due to its high efficiency caused by the strong affinity between the As and Fe at mild conditions of room temperature and pH[22,23]. Therefore, in this work were studied the equilibrium and kinetics of the adsorption process of arsenic ions on magnetite hollow nanoparticles (MNPs). The equilibrium study will provide relevant information related with the affinity between the adsorbate and adsorbent. The kinetics study will contribute with data associated with the time and concentration required to perform the removal process[24]. The experimental data was fitted with different kinetic models in order to set if the process was driven by physisorption or chemisorption. Additionally, several thermodynamic parameters such as the adsorption energy and Gibbs free energy were calculated.

* e-mail: patricia.amezaga@cimav.edu.mx

2. Experimental procedure

2.1. Synthesis and MNPs characterization

The MNPs were synthesized by the AACVD technique, details of the technique have been previously reported elsewhere[25-27]. Briefly, AACVD consists of an ultrasonic nebulizer, where the precursor solution is converted into a fine aerosol. The aerosol is transported into de furnace by the carrying gas. Once inside the furnace, the precursor solution contained in the aerosol is decomposed by effect of the thermal energy into the oxide, forming in it a fine powder on the walls of the tubular furnace. The precursor solution was a dilution of Fe (II) chloride in methanol (99.9%), at a concentration of 0.05 mol L^{-1}. The aerosol was carried by a mixture of Ar–air flow, (relation of 0.250:0.004 L min^{-1}, respectively). Synthesis temperature was fixed at 723 K. A collection flask was placed on super magnets with the function of attracting and collecting the MNPs obtained.

The microstructure of the pure MNPs and the MNPs-As was analyzed in two field emission microscopes, a scanning electron microscope (SEM) JEOL JSM-7401F and in a high resolution transmission electron microscope (HRTEM) JEOL JEM-2200FS. The elemental analysis was carried out by energy dispersive x-ray spectroscopy (EDS) attached to the column of the microscope. The EDS employed was an Inca from Oxford Instruments. Sample preparation consisted in dispersing the MNPs in ethanol and mixing under sonic conditions by 5 minutes. One drop of the solution was deposited on a Holey-Carbon Cu grid. Excess of ethanol was removed by drying under a visible light lamp. Prior to the introduction in the column the Cu-grid was cleaned with Plasma by 10 seconds.

MNPs-As were prepared as follows: first a solution of 500 ppm of arsenic in 100 ml of tridistilled water was prepared. Subsequently, 10 mg of MNPs were added to the solution and placed in ultrasonic agitation for 10 minutes. Once the time was elapsed, the solution was subjected to centrifugation at 5000 rpm by 15 minutes. Then the solution was decanted and separated from the collected MNPs-As. For the SEM analysis, the particles were dispersed in methanol by ultrasound for 1 minute, then three drops of the solution were deposited on a silicon substrate with an approximate area of 0.5 cm^2, and the substrate was allowed to dry. In this case, an elemental mapping for arsenic detection was performed on the MNPs-As. The specific surface area of MNPs was analyzed by the BET method before and after the contact with the arsenic to determine the amount of specific surface area being occupied by the ions of arsenic after the adsorption process.

2.2. Arsenic removal test

The arsenic ions precursors (99% purity, JT Baker) used in the preparation of solutions were sodium arsenite ($NaAsO_2$) and sodium arsenate dibasic heptahydrate ($Na_2HAsO_4{\cdot}7H_2O$), for the As^{+3} and As^{+5}, respectively. Two dilute solutions for each ion were prepared as: As^{+3} 0.152 and 0.164 mg L^{-1}, and As^{+5} 0.033 and 0.066 mg L^{-1}. To each of the dilute solutions were added 10 mg of MNPs and then left in contact under ultrasonic agitation. The contact times were 1, 5, 10, 15 and 30 minutes. After elapsed this time, in order to separating the MNPs from the liquid, the solutions were centrifuged at 5000 RPM by 10 minutes. Each clear solution was analyzed by atomic absorption spectroscopy (AAS, Avanta Sigma, GBC Scientific Equipment Ltd.) for determining the As and Fe content. The removal efficiency was calculated with equation (1), where C_0 is the initial As concentration in the solution prior to the contact test, and C_f is the As concentration determined from the AAS characterization:

$$Removal\ efficiency\ (\%) = [(C_0 - C_f)/C_0] \times 100 \quad (1)$$

2.3. Equilibrium study

2.3.1. Adsorption capacity

The adsorption capacity (q_e) was calculated from a mass balance according to equation (2), where C_o was the initial As concentration in the solution (mg L^{-1}), C_e the As concentration in the equilibrium (mg L^{-1}), V the volume of the solution (L) and M the mass of the MNPs (g).

$$q_e = [V * (C_0 - C_e)]/\mathrm{M} \quad (2)$$

2.3.2. Adsorption isotherms

The equilibrium adsorption isotherms provide useful information about the interactions between the adsorbate and the adsorbent. From this type of curves it was possible to determine the thermodynamic parameters and the maximum adsorption capacity. Several fitting models were tested (Langmuir[28], Freundlich[29] and Dubinin[30]) in order to find the best adjustment between the experimental data and the theoretical behavior. The models and the corresponding parameters are depicted in Table 1.

2.4. Adsorption process thermodynamics

2.4.1. Adsorption energy

The adsorption free energy (E) was determined to according to equation (3) and it represents the energy change required for transferring one mole of As ions from the solution onto the surface of the solid. If E is lower than 20 kJ mol^{-1} the adsorption process is called physisorption, if it is between 20-40 kJ mol^{-1} the process is known as ionic exchange, and when E is larger than 40 kJ mol^{-1} it is a chemisorption process. The Gibbs free energy (ΔG) indicates the energy required to displace the adsorbate onto the surface of the adsorbent[31] and was calculated according to equation (4).

$$E = \frac{1}{\sqrt{2K_D}} \quad (3)$$

$$\Delta G = RT\ Ln\frac{1}{K_L} \quad (4)$$

where K_D is the Dubinin constant, K_L is Langmuir constant, R is the universal gas constant (8.314 J mol^{-1} K^{-1}) and T is absolute temperature.

3. Results and discussion

3.1. Microstructure of the MNPS

Figure 1 (a-b) shows SEM micrographs of the MNPs synthesized by the AACVD method.

We can see particles with spherical morphology, each sphere is composed of crystallites, these particles tend to agglomerate, due to its size it is nanostructured. Two effects are observed when the size is reduced to nanostructured scale: a) a significant increase in surface area relative; b) a significant number of atoms on the surface increase. These effects increase the chemical reactivity of the surface of nanoparticles; this chemical reactivity and other properties depend on many factors: size, shape, chemical composition, electronic structure, surface structure, defects, diffusion, surface energy of the nanocrystals, interactions with atoms that are near and its chemical environment. The atoms on the surface of the nanoparticles are unstable, have a higher energy level and forces that are attracted by the atoms located inside the mass are very weak[53]. Therefore, by reducing the size at the nanoscale, the forces of Van der Waals attraction and its magnetic nature[25-27] of the nanostructures, increase and the spheres tend to attract each other and to form agglomerates. Most of the spherical particles consisted of crystallites with nanometric size, which formed the surface of the hollow sphere. The average particle size of the spherical particle was 300 ± 78 nm. Once analyzed, the MNPs were added to the arsenic solution and the results obtained by SEM show any change in the morphology of the nanoparticles (It is called nanoparticle because the sphere is formed of crystallites with size average of 20 nm, this means that the requirement of having at least 100 nm in size in one dimension is fulfilled, therefore, it can be mentioned as nanoparticle) after the adsorption of arsenic (Figure 1b). Figure 2 (a-b) shows a micrograph obtained by HRTEM of a single MNP and the corresponding elemental mapping determined by EDS . In Figure 2b the white dots forming the image of the particle indicated the presence of arsenic. It was observed a homogeneous distribution of the As adsorbed on the MNPs. With this, the adsorption of As by the MNPs was confirmed. However, the As was preferentially adsorbed on the crust of the particle rather than in the bulk. Figure 3 shows the EDS analysis performed on several of the MNPs. As expected, the quantification of the elements showed the presence of a high concentration of Fe and O, originated from the MNPs. The C, Si and Cu detected were originated from the elements conforming the support where the MNPs were deposited. The relatively low concentration of As was evidently produced by the adsorption of the ions on the surface of MNPs. Figure 4 shows the micrograph obtained by HRTEM and the corresponding line scan of elementes (Fe, O and As) determiend by EDS. With the line scans it was possible to determine the overall As distribution on the surface of a single MNP. These results suggested that most of the crystals forming the MNP contributed in the adsorption process, attraping several As ions[32,33].

Table 1: Models and parameters employed for fitting the adsorption isotherms in the equilibrium.

Isotherm	General Equation	Linearized equation	Parameters	Description
Langmuir	$q_e = \frac{Q_0 K_L C_e}{C_e K_L + 1}$	$\frac{C_e}{q_e} = \frac{C_e}{Q_0} + \frac{1}{K_L Q_0}$	Q_0	Maximum adsorption capacity
			K_L	Constant Langmuir (Adsorption energy)
			C_e	Equilibrium concentration of the As
			q_e	Equilibrium adsorption capacity of adsorbent
Freundlich	$q_e = Q_0 C_e^{\frac{1}{K_F}}$	$\ln(q_e) = \ln(Q_0) + \frac{1}{K_F}\ln(C_e)$	Q_0	Maximum adsorption capacity
			K_F	Constant Freundlich (Adsorption energy)
			C_e	Equilibrium concentration of the solution
Dubinin	$q_e = Q_0 e^{k\varepsilon^2}$	$\ln(q_e) = \ln(Q_0) - K_D\varepsilon^2$ $\varepsilon = RT\ln\left(1 + \frac{1}{C_e}\right)$	Q_0	Maximum adsorption capacity
			K_D	Free energy of the adsorption per molecule
			q_e	Equilibrium adsorption capacity of adsorbent
			R	Universal gas constant
			ε	Polanyi potential
			T	Ambient Temperature

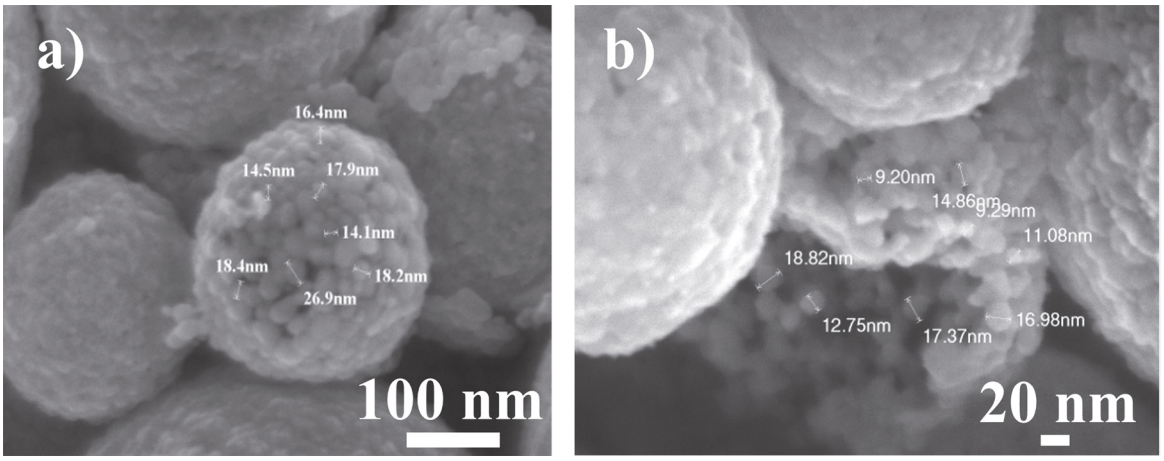

Figure 1: SEM images showing a) the morphology of the MNPs before arsenic adsorption process. b) Morphology of MNPs after the arsenic adsorption process.

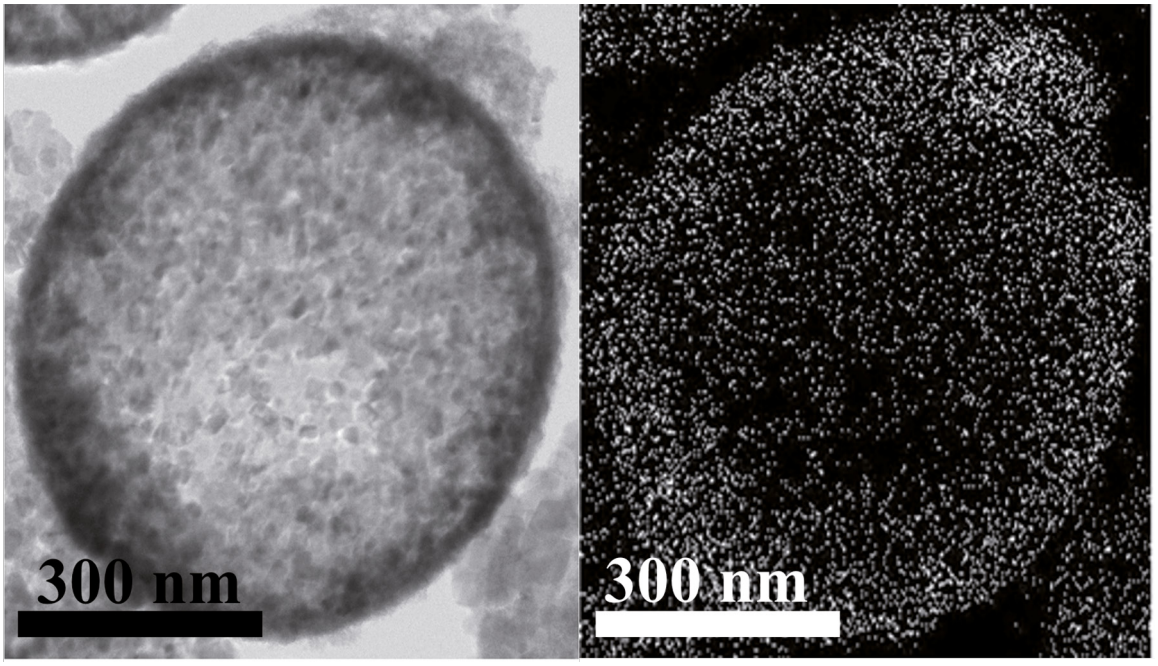

Figure 2: HRTEM image from a single MNP and Elemental mapping of a single MNPs. The scattered white dots indicate the distribution of the As ions on the MNPs.

3.2. Surface area measurements

The surface area calculated for MNPs before and after the adsorption process was 92 and 84 m^2/g respectively. The difference between these two measurements (8.7%) indicated that this value was the surface area occupied by arsenic. It is evident that the adsorption capacity depends largely on the specific surface area of the adsorbent and the affinity between the adsorbate and adsorbent. Altough the adsorbed As covered only a 8.7% of the surface of the particles, there still a large surface area where As ions may be adsorbed. This indicates the existence of free active sites for adsorbing more As ions i.e. in a continuos adsorption process.

3.3. Effect of contact time and solution concentration

Figure 5 shows the plots of the removal efficiency against the contact time of As ions (As^{+5} and As^{+3}) solutions at the different concentration. The curves showed a similar adsorption behavior. At early stages of the contact time, there was a high adsorption rate of As on the MNPs, which was caused by the large amount of available sites for As adsorption[34]. As the contact time elapsed, the active sites are being saturated with more As ions; this was observed as the decrease in the adsorption rate until the adsorption equilibrium is reached[35]. For the systems studied in this work,

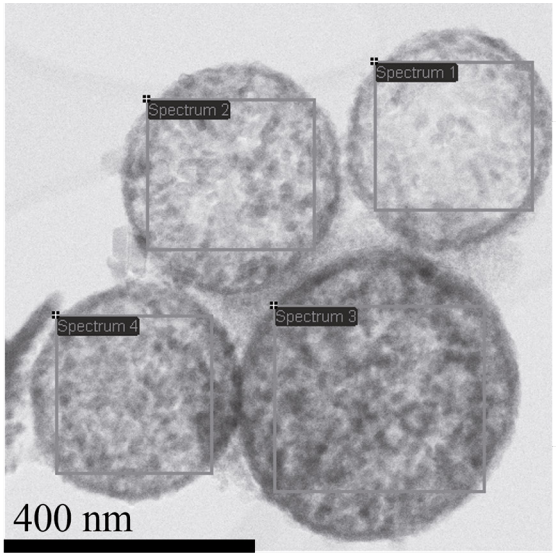

	Atomic %			
Elemento	S1	S2	S3	S4
C	12.45	13.53	16.34	9.54
O	49.18	48.82	45.15	51.30
Si	0.89	1.39	1.6	0.73
Fe	36.45	35.69	36.7	38.01
As	1.03	0.57	0.21	0.43
Total	100	100	100	100

Figure 3: EDS analyses from the MNPs synthesized by the AACVD method, after the contact tests with As ions (As^{+3} y As^{+5}).

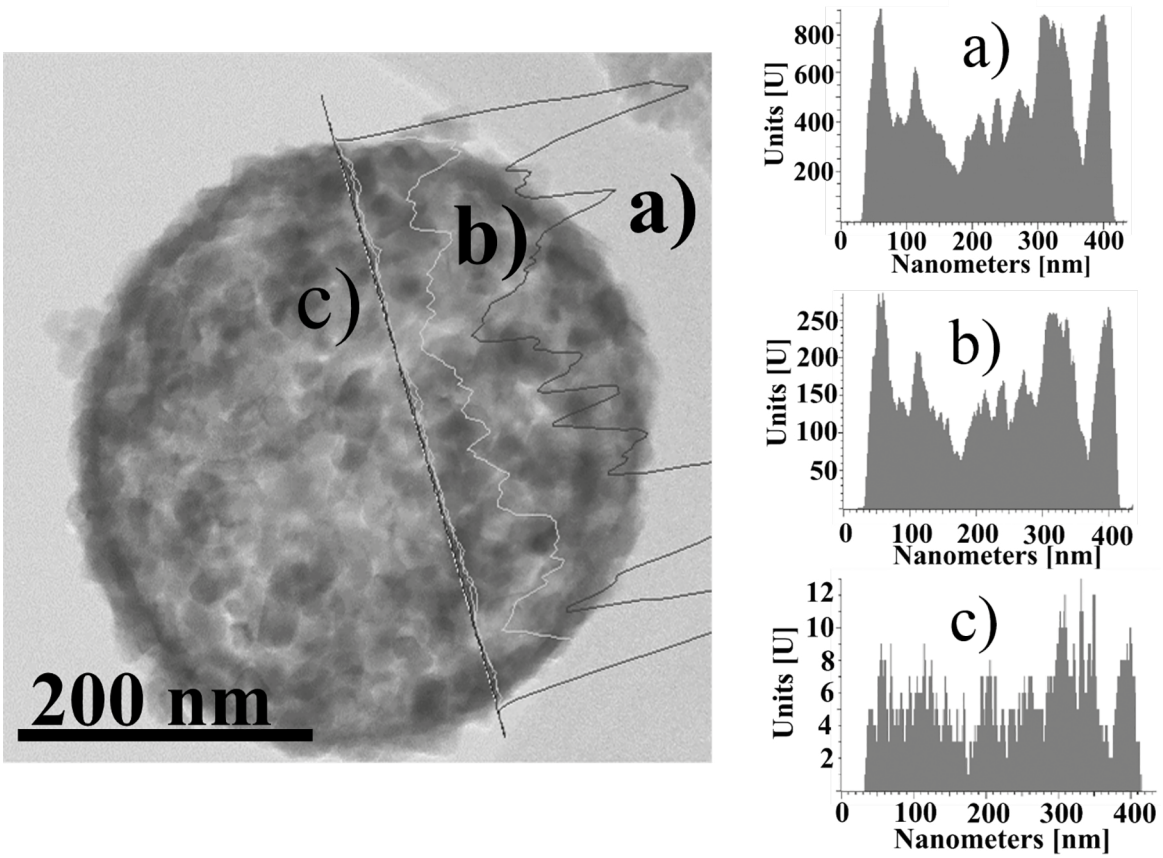

Figure 4: Scanning line by HRTEM, indicates the elemental distribution of As, O and Fe in MNPs.

the equilibrum was attached after 15 minutes of contact time. These results were similar to those previously reported by Naushad et al.[2,36] who found that the rate of adsorption was higher in the early stages of the removal process and then tend to decrease when the process reached the state of equilibrium. Table 2 shows the calculated removal efficiency (%) of As ions. As observed, for As^{+5} ions after 10 minutes of contact time it was reached an efficiency of 95%, while

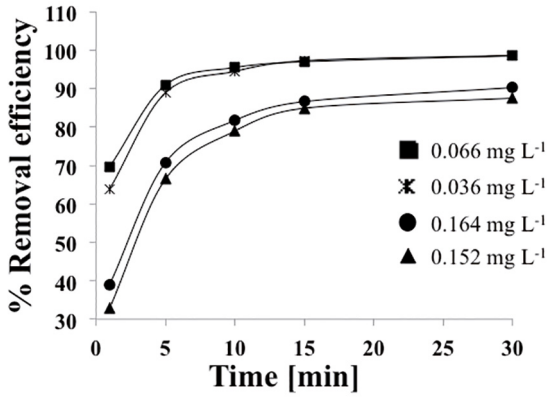

Figure 5: The removal efficiency of the As ions at different contact time.

As^{+3} ions after 15 minutes of contact time reached only 87%. These efficiency values were of importance since at these levels it was fulfilled the maximun concentration of As in water allowed in the international health standards. After 30 minutes of contact time As^{+5} ions were fully removed from the solution, while As^{+3} ions were removed only at 90%. Clearly, these suggested differences in the adsorption mechanism between the As^{+5} and As^{+3} ions. Commonly, prior to the removal of As^{+3} ions, these must be oxidized into As^{+5}. However, in the adsorption experiments performed in this work, As^{+3} ions were removed from water at a relative high efficiency without any previous treatment.

The mechanism of adsorption of As ions on FeOH was previoulsy reported by Xu et al.[37], Westeroff et al.[38] and Eby[39], and it was depicted in Figure 6. Results showed that only 10 mg of MNPs were enough to reach those removal eficiencies. The advantages of employing this type of MNPs are the low contact time required to achieve a high removal efficiency[40,41] and the prevention in the generation of residual sludge, which reduce the overall cost of the water treatment process.

3.4. Adsorption isotherms

Adsorption isotherms were constructed in order to show the adsorption capacity of the MNPs in the equilibrium. Table 3 shows the experimental conditions and the results of the calculated adsorption capacity (q_e). As observed in Table 3, the adsorption capacity increased with the initial concentration of the As solution; this was observed for both of the As ions tested. This behavior was explained in terms of the high mass transfer velocity produced by the larger amount of adsorbate available in the more concentrated solution[3,42,43]. Table 4 shows a summary of the results reported in literature of the adsorption capacities obtained with different types of adsorbents[44-46]. As can be infered, the adsorption capacity of the adsorbatent depends on the initial concentration of the adsorbeate, and in consequence the saturation point or equilibrium may be shifted in any direction. The experimental data describing the interactons solute-adsorbate was calculated from the fitting of the different models. Table 5 shows the results of the linnear regresion according to the Langmuir model. The monolayer content level (Q_0) represents the mass of ions adsorbed on the MNPs and forming a single monolayer of As ions[47-36]. Since in every case, the q_e values is larger than the Q_0, then it was suggested the formation of several layers adsorbed on the initial monolayer. This is a typical performance observed in physisorption processes. The calculated Lagmuir constant (K_L) can be interpred as the enthalpy of adsorption, showed negative values. This suggested the exothermal nature of the process and indicated that the surface of the MNPs was energetically favorable to react with the As ions. Table 6 shows the results of the Freundlich model. According to Mandal S. et al.[48,49], at higher K_F value will be higher the adsorption capacity of the adsorbent. Additionally, a K_F value higher than the unit indicates the spontaneous nature of the process [50]. In terms of the adsorption capacity, these results agreed with those calculated by the Langmuir model. However, for all the adsorption ishoterms, the regression coeficient (R^2) was more reliable for the Freundlich model than for the Langmuir model. Table 7 shows the results obtained after applying the Dubinin model. The regression coefficent was similar to those calculated by the Freundlich model, and the Q_0 value was lower than the q_e value, confirming the formation of several adsorbed layers of As ions during the adsorption process [2].

3.5. Determination of adsorption energy and Gibbs free energy

Tables 8 and 9 show the results of the adsorption free energy and Gibbs free energy, calculated from the Dubinin and Langmuir constants, respectively. The results indicated that the energy required to transfer one mole of

Table 2: Results of the removal of As ions (As^{+3} y As^{+5}) from water. The initial concentration of As in the solution is indicated in square brackets.

Time (min)	As^{+5} removal (%) [0.036 mg L^{-1}]	As^{+5} removal (%) [0.066 mg L^{-1}]	As^{+3} removal (%) [0.152 mg L^{-1}]	As^{+3} removal (%) [0.164 mg L^{-1}]
1	64	70	49	54
5	89	91	62	68
10	94	95	73	78
15	96	98	85	87
30	100	100	88	90

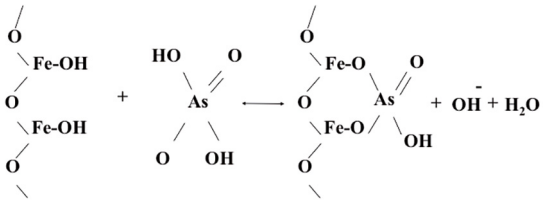

Figure 6: Proposed mechanism of arsenic adsorption process by MNPs[37-39].

Table 3: Experimental conditions employed in the contact adsorption tests for calculating the adsorption capacity.

	C_0 (mg L^{-1})	V (L) Solution	MNPs (mg)	q_e (mg g^{-1})
As^{+5}	0.036	0.1	0.01	0.355
As^{+5}	0.066	0.1	0.01	0.63
As^{+3}	0.152	0.1	0.01	1.33
As^{+3}	0.164	0.1	0.01	1.38

As ions from the solution onto the surface of the adsorbate (MNPs) was very close to 20 kJ mol^{-1} for the As^{+5} and 7.6 kJ mol^{-1} for the As^{+3}. These values corroborated that the interactions among the adsorbate and the adsorbent were of the physical type, i.e. physisorption process[51,52]. The calculated Gibbs free energy for the both. As ions presented a negative value, indicating the spontaneous nature of the process. Furthermore, as the concentration of the solution decreased, the calculated value of the energies (E and ΔG) was more negative, indicating that the physisorption process was more favorable. These results were similar to those reported by Naushad et al.[52]. Furthermore, when the concentration of the adsorbate in the solution decreased, the calculated value for the energies (*E* and ΔG) also decreases, indicating that the physisorption process was more favorable.

4. Conclusions

The study presented herein showed that the hollow magnetic nanoparticles (MNPs) can be employed as a promising material in the removal of As ions (As^{+5} and As^{+3}) from water. The adsorption experiments showed that As ions could be removed with a high efficiency (90%) in a relatively short time (15 minutes). From the high resolution electron microscopy images, it was observed that the As ions were adsorbed and well distributed on the surface of the MNPs. Several physical models were employed to fit the experimental data and the results indicated the formation of several layers of As ions on the MNPs. The calculated adsorption free energy and Gibbs free energy indicated that the adsorption process was conducted by physisorption (E < 20 kJ mol^{-1}) and spontaneously (ΔG < 0). From the three models fitted (Langmuir, Freundlich and Dubinin), Langmuir showed the lower regression coefficients, but the three models agreed very well in predicting the adsorption capacity.

Table 4: Adsorption capacities of different types adsorbents, with different amounts of adsorbate and adsorbent.

Adsorbent	Initial concentration of adsorbate	Adsorption capacity (mg g^{-1})	Amount of Adsorbent utilized
Nickel/nickel boride nanoparticles coated resin [4]	100 ppm	23.4 As^{+3} 17.8 As^{+5}	0.1 g 0.4 g
Fe_7S_8 nanoparticles[5]	300 ppb	14.3 As^{+3} 31.3 As^{+5}	0.01g
Iron oxide Green nanoparticles[44]	600 ppm	3.77 As^{+5}	2.5 g
MOF-808 nanoparticles[45]	5 ppm	24.83 As^{+5}	0.01 g
TiO_2 nanoparticles[46]	0.1 ppm	3.1 As^{+5}	0.2 gr
Magnetite nanoparticles (this work)	0.066 ppm 0.134 ppm	0.63 As^{+5} 1.38 As^{+3}	0.01 g

Table 5: Results from the Langmuir model for the adsorption of As ions (As^{+3} y As^{+5}) on the MNPs.

	As^{+5}		As^{+3}	
	Concentration 0.036 mg L^{-1}	Concentration 0.066 mg L^{-1}	Concentration 0.152 mg L^{-1}	Concentration 0.164 mg L^{-1}
Adsorption capacity of a monolayer Q_0 (mg g^{-1})	0.338	0.623	1.052	1.219
Langmuir constant K_L (L mg^{-1})	-37	-23	-2.4	-1.9
Adsorption capacity q_e (mg g^{-1})	0.35	0.63	1.33	1.38
Regression coefficient R^2	0.85	0.91	0.97	0.95

Table 6: Results from the Freundlich model for the adsorption of As ions (As^{+3} y As^{+5}) on the MNPs.

	As^{+5}		As^{+3}	
	Concentration 0.036 mg L^{-1}	Concentration 0.066 mg L^{-1}	Concentration 0.152 mg L^{-1}	Concentration 0.164 mg L^{-1}
Adsorption capacity of a monolayer Q_0 (mg g^{-1})	0.28	0.54	0.610	0.77
Freundlich constant K_F (L mg^{-1})	-32	-36	-5	-6.3
Adsorption capacity q_e (mg g^{-1})	0.35	0.63	1.33	1.38
Regression coefficient R^2	0.97	0.96	0.98	0.99

Table 7: Results from the Dubinin model for the adsorption of As ions (As^{+3} y As^{+5}) on the MNPs.

	As^{+5}		As^{+3}	
	Concentration 0.036 mg L^{-1}	Concentration 0.066 mg L^{-1}	Concentration 0.152 mg L^{-1}	Concentration 0.164 mg L^{-1}
Adsorption capacity of a monolayer Q_0 (mg g^{-1})	0.278	0.528	0.439	0.606
Dubinin constant K_D (L mg^{-1})	0.0013	0.0012	0.011	0.0086
Adsorption capacity q_e (mg g^{-1})	0.35	0.63	1.33	1.38
Regression coefficient R^2	0.96	0.97	0.99	0.99

Table 8: Adsorption free energy for As ions (As^{+5} y As^{+3}) at different experimental conditions, calculate from the Dubinin model

As ion	Concentration (mg L^{-1})	Dubinin Constant (mol^2 kJ^{-2})	Adsorption free Energy (kJ mol^{-1})
As^{+5}	0.036	0.0013	19
As^{+5}	0.066	0.0012	20
As^{+3}	0.152	0.0011	6.7
As^{+3}	0.164	0.0086	7.6

Table 9: Gibbs free energy for As ions (As^{+5} y As^{+3}) at different experimental conditions, calculate from the Langmuir model

As ion	Concentration (mg L^{-1})	Langmuir Constant (mol^2 kJ^{-2})	Adsorption free energy (kJ mol^{-1})
As^{+5}	0.036	37	-8.8
As^{+5}	0.066	23	-7.6
As^{+3}	0.152	2.4	-2.14
As^{+3}	0.164	1.9	-1.57

5. Acknowledgements

Authors thank to S. Miranda, A. Benavidez, P. Peregrino, C. Ornelas, O. Esquivel-Pereyra, A. Heiras-Trevizo, G. Romero-Rubio for the technical assistance provided during the realization of this work. This work was partially supported by a grant from CONACYT PDCPN2014-01 Project 248289.

6. References

1. Naushad M, ALOthman ZA, Awual MR, Alam MM, Eldesoky GE. Adsorption kinetics, isotherms, and thermodynamic studies for the adsorption of Pb^{2+} and Hg^{2+} metal ions from aqueous medium using Ti(IV) iodovanadate cation exchanger. *Ionics*. 2015;21(8):2237-2245.

2. Naushad M, Ansari AA, ALOthman ZA, Mittal J. Synthesis and characterization of YVO_4:Eu^{3+} nanoparticles: kinetics and isotherm studies for the removal of Cd^{2+} metal ion. *Desalination and Water Treatment*. 2014;57(5):2081-2088.

3. Fernández-López JA, Angosto JM, Avilés MD. Biosorption of Hexavalent Chromium from Aqueous Medium with *Opuntia Biomass*. *The Scientific World Journal*. 2014;2014:670249.

4. Çiftçi TD, Henden E. Nickel/nickel boride nanoparticles coated resin: A novel adsorbent for arsenic(III) and arsenic(V) removal. *Powder Technology*. 2015;269:470-480.

5. Cantu J, Gonzalez LE, Goodship J, Contreras M, Joseph M, Garza C, et al. Removal of arsenic from water using synthetic Fe_7S_8 nanoparticles. *Chemical Engineering Journal*. 2016;290:428-437.

6. Jain CK, Ali I. Arsenic: occurrence, toxicity and speciation techniques. *Water Research*. 2000;34(17):4304-4312.

7. Zhang S, Niu H, Cai Y, Zhao X, Shi, Y. Arsenite and arsenate adsorption on coprecipitated bimetal oxide magnetic nanomaterials: $MnFe_2O_4$ and $CoFe_2O_4$. *Chemical Engineering Journal*. 2010;158(3):599-607.

8. México. Secretaría de Salud. *Norma Oficial Mexicana NOM-127-SSA1-2015, Salud ambiental. Agua para uso y consumo humano. Límites permisibles de calidad y tratamientos a que debe someterse el agua para su potabilización*. Ciudad de México: Secretaría de Salud; 2015,

9. Malana MA, Qureshi RB, Ashiq MN. Adsorption studies of arsenic on nano aluminium doped manganese copper ferrite polymer (MA, VA, AA) composite: kinetics and mechanism. *Chemical Engineering Journal*. 2011;172(2-3):721-727.

10. Kundu S, Gupta AK. Arsenic adsorption onto iron oxide-coated cement (IOCC): Regression analysis of equilibrium data with several isotherm models and their optimization. *Chemical Engineering Journal.* 2006;122(1-2):93-106.

11. Manning BA, Goldberg S. Arsenic (III) and arsenic (V) adsorption on three California soils. *Soil Science.* 1997;162(12):886-895.

12. Borho M, Wilderer P. Optimized removal of arsenate (III) by adaptation of oxidation and precipitation processes to the filtration step. *Water Science and Technology*. 1996;34(9):25-31.

13. Hansen HK, Nuñez P, Grandon R. Electrocoagulation as a remediation tool for wastewaters containing arsenic. *Minerals Engineering*. 2006;19(5):521-524.

14. Han B, Runnells T, Zimbron J, Wickramasinghe R. Arsenic removal from drinking water by flocculation and microfiltration. *Desalination*. 2002;145(1-3):293-298.

15. Kim J, Benjamin MM. Modeling a novel ion exchange process for arsenic and nitrate removal. *Water Research*. 2004;38(8):2053-2062.

16. Benjamin MM, Sletten RS, Bailey RP, Bennett T. Sorption and filtration of metals using iron-oxide-coated sand. *Water Research*. 1996;30(11):2609-2620.

17. Martinson CA, Reddy KJ. Adsorption of arsenic(III) and arsenic(V) by cupric oxide nanoparticles. *Journal of Colloid and Interface Science*. 2009;336(2):406-411.

18. Manning BA, Fendorf SE, Bostick B, Suarez DL. Arsenic(III) Oxidation and Arsenic(V) Adsorption Reactions on Synthetic Birnessite. *Environmental Science & Technology*. 2002;36(5):976-981.

19. Liu Z, Zhang FS, Sasai R. Arsenate removal from water using Fe_3O_4-loaded activated carbon prepared from waste biomass. *Chemical Engineering Journal*. 2010;160(1):57-62.

20. Xu Z, Li Q, Gao S, Shang JK. As(III) removal by hydrous titanium dioxide prepared from one-step hydrolysis of aqueous $TiCl_4$ solution. *Water Research*. 2010;44(19):5713-5721.

21. Kanel SR, Grenèche JM, Choi H. Arsenic(V) Removal from Groundwater Using Nano Scale Zero-Valent Iron as a Colloidal Reactive Barrier Material. *Environmental Science & Technology*. 2006;40(6):2045-2050.

22. Korngold E, Belayev N, Aronov L. Removal of arsenic from drinking water by anion exchangers. *Desalination*. 2001;141(1):81-84.

23. Dambies L, Salinaro R, Alexandratos SD. Immobilized *N*-Methyl-D-glucamine as an Arsenate-Selective Resin. *Environmental & Science Technology*. 2004;38(22):6139-6146.

24. Ho YS, Ng JCY, McKay G. Kinetics of pollutant sorption by biosorbents: Review. *Separation & Purification Reviews*. 2000;29(2):189-232.

25. Monárrez-Cordero B, Amézaga-Madrid P, Antúnez-Flores W, Leyva-Porras C, Pizá-Ruiz P, Miki-Yoshida M. Highly efficient removal of arsenic metal ions with high superficial area hollow magnetite nanoparticles synthetized by AACVD method. *Journal of Alloys and Compounds*. 2014;586(Suppl 1):S520-S525.

26. Monárrez-Cordero BE, Amézaga-Madrid P, Hernández-Salcedo PG, Antúnez-Flores W, Leyva-Porras C, Miki-Yoshida M. Theoretical and experimental analysis of the aerosol assisted CVD synthesis of magnetite hollow nanoparticles. *Journal of Alloys and Compounds*. 2014;615(Suppl 1):S328-S334.

27. Hernández-Salcedo PG, Amézaga-Madrid P, Monárrez-Cordero BE, Antúnez Flores W, Pizá-Ruiz P, Leyva-Porras C, et al. Theoretical and experimental influence of aerosol assisted CVD parameters on the microstructural properties of magnetite nanoparticles and their response on the removal efficiency of arsenic. *Journal of Alloys and Compounds*. 2014;643(Suppl 1):S287-S296.

28. Iqbal MJ, Ashiq MN. Adsorption of dyes from aqueous solution on activated charcoal. *Journal of Hazardous Materials*. 2007;139(1):57-66.

29. Renault F, Morin-Crini N, Gimbert F, Badot PM, Crini G. Cationized starchbased material as a new ion-exchanger adsorbent for the removal of C. I. Acid Blue 25 from aqueous solutions. *Bioresource Technology*. 2008;99(16):7573-7586.

30. Shrestha RR, Shrestha MP, Upadhyay NP, Pradhan R, Khadka R, Maskey A, et al. Groundwater arsenic contamination, its health impact and mitigation program in Nepal. *Journal of Environmental Science and Health Part A, Toxic/Hazardous Substances & Environmental Engineering*. 2003;38(1):185-200.

31. Maji SK, Pal A, Pal T. Arsenic removal from real-life groundwater by adsorption on laterite soil. *Journal of Hazardous Materials*. 2008;151(2-3):811-820.

32. Litter MI, Alarcón-Herrera MT, Arenas MJ, Armienta MA, Avilés M, Cáceres RE, et al. Small-scale and household methods to remove arsenic from water for drinking purposes in Latin America. *Science of The Total Environment*. 2012;429:107-122.

33. Wu FC, Tseng RL, Juang RS. Initial behavior of intraparticle diffusion model used in the description of adsorption kinetics. *Chemical Engineer Journal*. 2009;153(1-3):1-8.

34. Naushad M, ALOthman ZA. Separation of toxic Pb^{2+} metal from aqueous solution using strongly acidic cation-exchange resin: analytical applications for the removal of metal ions from pharmaceutical formulation. *Desalination and Water Treatment*. 2013;53(8):2158-2166.

35. Vadivelan V, Kumar KV. Equilibrium, kinetics, mechanism, and process design for the sorption of methylene blue onto rice husk. *Journal of Colloid and Interface Science*. 2005;286(1):90-100.

36. Naushad M, ALOthman ZA, Alam MM, Awual MR, Eldesoky GE, Islam M. Synthesis of sodium dodecyl sulfate-supported nanocomposite cation exchanger: removal and recovery of Cu^{2+} from synthetic, pharmaceutical and alloy samples. *Journal of the Iranian Chemical Society*. 2015;12(9):1677-1686.

37. Xu YH, Nakajima T, Ohki A. Adsorption and removal of arsenic(V) from drinking water by aluminum-loaded Sirasu-zeolite. *Journal of Hazardous Materials*. 2002;92(3):275-287.

38. Westerhoff P, Highfield D, Badruzzaman M, Yoon Y. Rapid small-scale column tests for arsenate removal in iron oxide packed bed columns. *Journal of Environmental Engineering*. 2005;131(2):262-271.

39. Nelson Eby G. Principles of Environmental Geochemistry. Pacific Grove: Brooks/Cole-Thomson Learning; 2004. 514 p.

40. Urbano BF, Rivas BL, Martinez F, Alexandratos SD. Equilibrium and kinetic study of arsenic sorption by water-insoluble nanocomposite resin of poly[N-(4-vinylbenzyl)-N-methyl-d-glucamine]-montmorillonite. *Chemical Engineering Journal*. 2012;193-194:21-30.

41. Garg UK, Kaur MP, Garg VK, Sud D. Removal of nickel(II) from aqueous solution by adsorption on agricultural waste biomass using a response surface mehodological approach. *Bioresource Technology*. 2008;99(5):1325-1331.

42. Karami H. Heavy metal removal from water by magnetite nanorods. *Chemical Engineering Journal*. 2013;219:209-216.

43. Alqadmi AA, Naushad M, Abdalla MA, Ahamad T, Alothman ZA, Alshehri SM. Synthesis and characterization of Fe_3O_4@TSC nanocomposite: highly efficient removal of toxic metal ions from aqueous medium. *RSC Advances*. 2016;6(27):22679-22689.

44. Saritha A, Raju B, Narayana RD, Roychowdhury A, Das D, Hussain KA. Facile green synthesis of iron oxide nanoparticles via solid-state thermolysis of a chiral, 3D anhydrous potassium tris(oxalato)ferrate(III) precursor. *Advanced Powder Technology*. 2015;26(2):349-354.

45. Li ZQ, Yang JC, Sui KW, Yin N. Facile synthesis of metal-organic framework MOF-808 for arsenic removal. *Materials Letters*. 2015;160:412-414.

46. Ramos MLP, González JA, Albornoz SG, Pérez CJ, Villanueva ME, Giorgieri SA, et al. Chitin hydrogel reinforced with TiO_2 nanoparticles as an arsenic sorbent. *Chemical Engineering Journal*. 2016;285:581-587.

47. Rodríguez Vidal FJ. *Proceso de filtración - adsorción y efecto del ozono. Procesos de potabilización del agua e influencia del tratamiento de ozonización*. 1er ed. Madrid: Díaz de Santos: 2006; 196 p.

48. Mandal S, Sahu MK, Giri AK, Patel RK. Adsorption studies of chromium (VI) removal from water by lanthanum diethanolamine hybrid material. *Environmental Technology*. 2014;35(7):817-832.

49. Naushad M, Khan M, ALOthman ZA, AlSohaimi I, Rodriguez-Reinoso F, Turki M, et al. Removal of BrO_3^- from drinking water samples using newly developed agricultural waste-based activated carbón and its determination by ultra-performance liquid chromatography-mass spectrometry. *Environmental Science and Pollution Research*. 2015;22(20):15853-15865.

50. Mandal S, Mahapatra SS, Patel RK. Neuro fuzzy approach for arsenic(III) and chromium(VI) removal from watery. *Journal of Water Process Engineering*. 2015;5:58-75.

51. Hokkanen S, Repo E, Lou S, Sillanpää M. Removal of arsenic(V) by magnetic nanoparticle activated microfibrillated cellulose. *Chemical Engineering Journal*. 2015;260:886-894.

52. Naushad M, ALOthman ZA, Sharma G, Inamuddin. Kinetics, isotherm and thermodynamic investigations for the adsorption of Co(II) ion onto crystal violet modified amberlite IR-120 resin. *Ionics*. 2015;21(5):1453-1459.

53. Cornejo-Alvarez L. La Revolución Nanotecnológica del Siglo XXI. Available from: <http://nuevastecnologiasymateriales.com/revolucion-nanotecnologia-siglo-xxi/>. Access in: 24/11/2016.